A Novel Low-Loss Diamond-Core Porous Fiber for Polarization Maintaining Terahertz Transmission

Raonaqul Islam, Md. Selim Habib, G. K. M. Hasanuzzaman, Sohel Rana, Md. Anwar Sadath, and Christos Markos

***Abstract*— We report on the numerical design optimization of a new kind of relatively simple porous-core photonic crystal fiber (PCF) for terahertz (THz) waveguiding. A novel twist is introduced in the regular hexagonal PCF by including a diamond-shaped porous-core inside the hexagonal cladding. The numerical results obtained from an efficient finite-element method, which confirms a high birefringence of the order 10^{-2} and low effective material loss of 0.07 cm^{-1} at 0.7-THz operating frequency. The proposed PCF is anticipated to be useful in polarization sensitive THz appliances.**

***Index Terms*— Birefringence, porous-core, photonic crystal fiber, terahertz wave guidance.**

I. Introduction

PHOTONIC crystal fibers (PCFs) are often considered as waveguiding solutions to the well-known terahertz (THz) technology. Since regular dielectrics absorb excessive power in this radiation band and dry air is transparent for THz waves, PCFs are so designed based on polymers that majority of the power fraction is guided in air-holes. Convenient porous fibers with air-cladding [1] and porous fibers with holey cladding [2], [3] have been reported earlier, where most of the power was propagated in low-loss air.

Meanwhile, significant applications such as THz time domain spectroscopy [4], [5] require polarization maintenance in the THz regime. Symmetry of a PCF is deliberately defected to induce high modal birefringence for THz polarization maintaining applications [6]–[10]. For example, Cho *et al.* demonstrated a plastic PCF [6] that exhibits a birefringence as high as 2.1×10^{-2}. However, the high propagation loss 400 dB/m at 1 THz makes the waveguide impractical for low-loss THz guiding. Use of rectangular air-holes [7], [8] or elliptical air-holes [9], [10] in the core one can achieve high-birefringence in the order 10^{-2}. Nevertheless, the complicated rectangular or elliptical shapes introduce difficulty in practical realization of these structures and transmission loss is yet high due to absorption in the solid material. Moreover, these structures [7]–[10] use solid air-cladding that involves direct connection with the outer environment where uncertain atmospheric losses may occur.

In this letter, we propose a simple and novel diamond-core PCF that shows simultaneously a high-birefringence of $\sim 10^{-2}$ and a low effective absorption loss of ~ 0.07 cm^{-1} for both the polarization modes. Most importantly, it does not include any complex shaping and only circular air-holes are considered for the structure. To the best of our knowledge, this type of PCF has never been conferred in the THz research before.

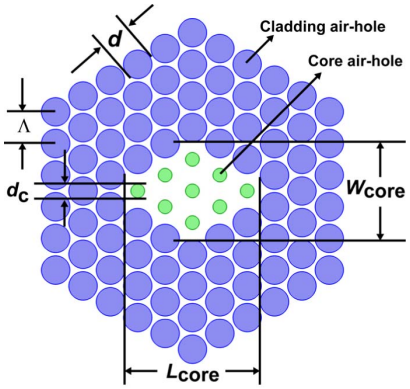

Fig. 1. Schematic diagram of the proposed diamond-core fiber structure.

II. Design Methodology

Fig. 1 shows the cross-section of the diamond-core structure. The core consists of diamond shape of air-hole pattern (green circles) whereas the cladding consists of regular hexagonal air-hole pattern (blue circles). The diameter of the core air-holes (d_c) was reduced compared to the diameter of the cladding air-holes (d) in order to create the differential index contrast between the core and the cladding. Meanwhile, the principle design parameter chosen for this design is the length of the diamond-core (L_{core}) because it determines the fiber dimension. The width of the core (W_{core}) changes according to the L_{core}. The pitch (Λ), in other words, the distance between two adjacent air-holes of the same ring and two different rings throughout the structure, is related to L_{core} as $L_{core} = 6\Lambda \cos 30^\circ - d$. That means we set the value of L_{core} to find out the pitch of the fiber. The air-filling ratio (d/Λ)

Manuscript received July 18, 2015; revised December 10, 2015; accepted March 31, 2016. Date of publication April 6, 2016; date of current version May 16, 2016.

R. Islam, G. K. M. Hasanuzzaman, S. Rana, and M. A. Sadath are with the Department of Electrical and Electronic Engineering, Rajshahi University of Engineering and Technology, Rajshahi 6204, Bangladesh (e-mail: raonaq.i@gmail.com; g.kibria82@yahoo.com; sohel271679rana@gmail.com; bidduth08@yahoo.com).

M. S. Habib is with the Department of Electrical and Electronic Engineering, Rajshahi University of Engineering and Technology, Rajshahi 6204, Bangladesh, and also with the Department of Photonics Engineering, Technical University of Denmark, Kongens Lyngby 2800, Denmark (e-mail: seha@fotonik.dtu.dk).

C. Markos is with the Department of Photonics Engineering, Technical University of Denmark, Kongens Lyngby 2800, Denmark (e-mail: chmar@fotonik.dtu.dk).

Color versions of one or more of the figures in this letter are available online at http://ieeexplore.ieee.org.

Digital Object Identifier 10.1109/LPT.2016.2550205

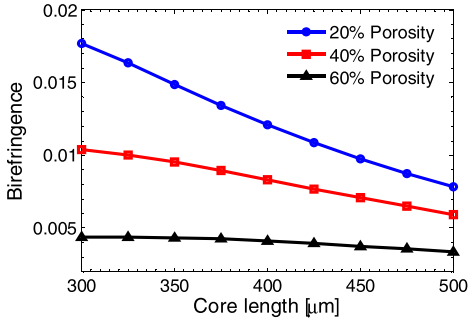

Fig. 2. Birefringence as a function of core length for different porosities at 1 THz.

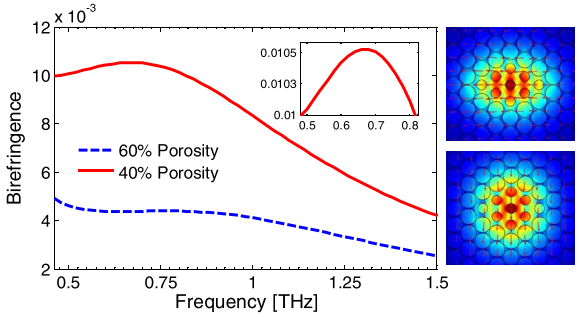

Fig. 3. Birefringence versus frequency. Right hand side shows electric field distribution of the fundamental mode for x-polarization mode (top) and y-polarization mode (bottom) at $L_{\text{core}} = 400$ μm, 40% porosity and 0.7 THz.

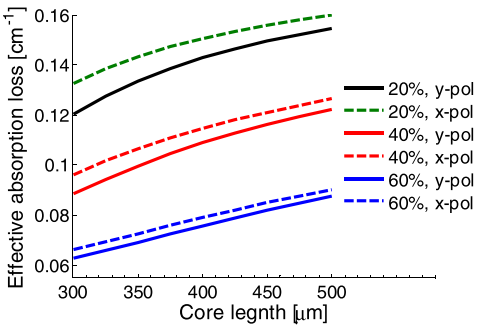

Fig. 4. Effective material absorption loss versus core length at 1 THz.

of the cladding is kept fixed at 0.95 throughout the analysis. We have defined the core porosity as the ratio between core air-hole areas to the total core area.

The background material considered for this design is cyclic olefin copolymer (COC), with a trade name of TOPAS. This polymer is preferred due to some of its excellent merits over other polymers such as PMMA or Teflon. For example, its refractive index is constant between 0.1-2 THz [11], its bulk material loss is very low compared to other polymers ($\sim$0.2 cm^{-1} at 1 THz) [11], it is humidity insensitive [12], and good for biosensing [13]. An efficient finite element method (FEM) based commercially available state-of-the-art *COMSOL* has been used to compute the modal properties of the proposed PCF. In addition, a perfectly matched layer (PML) is applied outside the computational domain to model the loss properties. The overall computational domain was 525 μm when length of the diamond-core, L_{core} was 400 μm. We used 21382 triangular vector edge elements and 3086 PML boundary elements to represent the structure, whereas the average element quality of the fiber was $\sim$0.9404 which confirms the computational error less than 0.1%.

III. Results and Discussion

First, we demonstrate the birefringence of the proposed fiber. Birefringence is basically the absolute difference between the refractive indices of x and y polarization modes expressed as [10]

$$B = \left| n_{\text{x}} - n_{\text{y}} \right|, \tag{1}$$

where B stands for birefringence, n_{x} and n_{y} indicate effective refractive indices of x and y polarization modes respectively. Fig. 2 shows the calculated birefringence as a function of the core length at 20%, 40% and 60% core porosities. Apparently, birefringence is reduced when porosity is increased, whereas the variation of birefringence over core length is increased when the porosity is reduced. This happens because increment of porosity reduces the differential index contrast between the core and the cladding, resulting in less power inside the porous-core. As a consequence, the deliberate stress on the guided mode introduced by the diamond-core is decreased and thus birefringence is reduced. The birefringence for 20% porosity within 300-450 μm and for 40% porosity within 300-325 μm at 1 THz are high ($>10^{-2}$), which are comparable to the previously published works [6]–[10]. The proposed fiber shows high-birefringence despite being exclusive of elliptical or rectangular shapes, which we believe will give a tremendous advantage from fabrication point of view. The diamond-core structure can be realized more clearly from Fig. 3 in which the birefringence is illustrated as a function of frequency. It can be observed from Fig. 3 that for 40% porosity, the proposed design shows high-birefringence ($>10^{-2}$) within a wide frequency band (0.48-0.82 THz). To be specific, at 0.7 THz and 40% porosity, the birefringence is maximum (0.0105) for this design. The fundamental mode field pattern is also shown in Fig. 3 where mode field is well confined inside the core.

We now discuss the most important loss in the THz regime which is effective absorption loss, expressed as [3]

$$\alpha_{\text{eff}} = \sqrt{\frac{\varepsilon_0}{\mu_0}} \left(\frac{\int_{\text{mat}} n_{\text{mat}} \left| E \right|^2 \alpha_{\text{mat}} \text{dA}}{\left| \int_{\text{all}} S_{\text{z}} \text{dA} \right|} \right), \tag{2}$$

where ε_{o} and μ_{o} are the permittivity and permeability of vacuum, n_{mat} is the refractive index of the material used, E is the modal electric field, α_{mat} is the bulk material absorption loss and S_{z} is the z-component of the Poynting vector, $S_{\text{z}} = \frac{1}{2}\left(\vec{E} \times \vec{H}\right) \cdot \hat{z}$. The effective absorption loss as a function of core length of the proposed design is plotted in Fig. 4, where it is observed that the two polarization modes show different absorption loss and the loss is increased when porosity is reduced. The amount of absorbed power also increases with the frequency as shown in Fig. 5. This demonstration is performed after considering the incremental bulk-material loss of TOPAS with respect to the frequency as described in Ref. [7]. Although 60% porosity shows lower absorp-

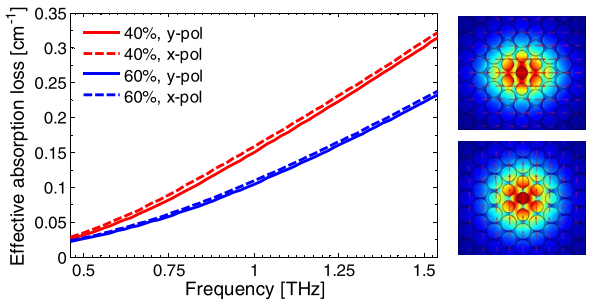

Fig. 5. Effective absorption loss versus frequency. Right hand side shows electric field distribution of the fundamental mode for x-polarization mode (top) and y-polarization mode (bottom) at $L_{\text{core}} = 400$ μm, 60% porosity and 1 THz.

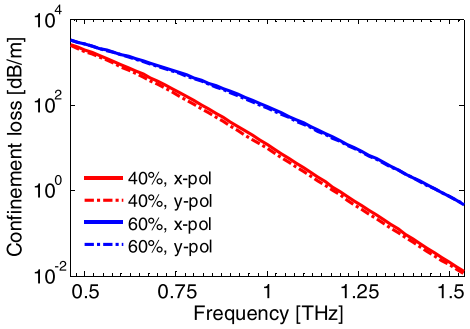

Fig. 6. Confinement loss versus core length for different porosities at 1 THz.

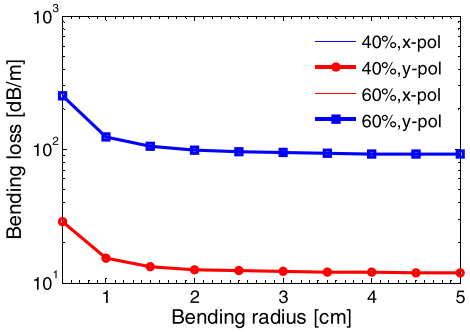

Fig. 7. Bending loss versus bending radius for different porosities and different polarization modes. Note that the bending loss for both polarization modes overlap each other.

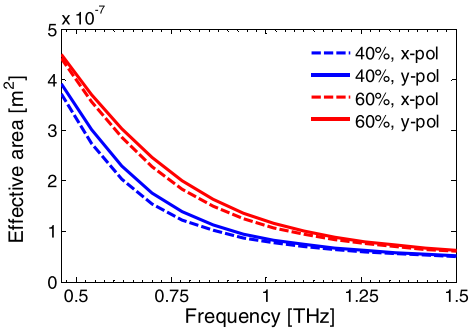

Fig. 8. Effective area as a function of frequency for different.

tion loss than 40% (Fig. 5), the porosity dependent loss is very low in the high-birefringence frequency band of interest 0.48-0.82 THz. Please note that the loss is 0.07 cm^{-1} for y-polarized mode and 0.076 cm^{-1} for x-polarized mode at 40% porosity and 0.7 THz, which is the clinical evidence of low polarization dependent loss. This can be understood more clearly from the fundamental mode field pattern in Fig. 5, which show that most of the power is propagated in air-holes for both the polarization modes. It is worthwhile to mention that the loss obtained at 40% porosity and 0.7 THz is lower than the earlier reported ones [2], [3], [6]–[10]. Next, we analyze the confinement loss of the fiber which is expressed as [14]

$$\alpha_{\text{CL}} = 8.686 k_0 \text{Im}(n_{\text{eff}}), \tag{3}$$

where $k_0 = 2\pi/\lambda$ and $\text{Im}(n_{\text{eff}})$ is the imaginary part of the refractive index, n_{eff}. Fig. 6 shows the confinement loss property of the proposed fiber with respect to frequency. We observe that confinement loss is increased when frequency is decreased to the band of interest (0.48-0.82 THz). Most importantly, the polarization dependent loss is low for all porosities (Fig. 6), which is of utmost importance for high-birefringence polarization maintenance.

To calculate the bending loss, first we replace the bent fiber with its equivalent straight fiber. Then the effective refractive index of that fiber is found from the conformal transformation method which is used to calculate the leakage loss. The equivalent refractive index is given by [15], [16]

$$n_{\text{eq}}(x, y) = n(x, y) \exp(1 + x/R), \tag{4}$$

where, $n(x, y)$ is the original refractive index profile of the fiber, R is the bending radius and x is the distance from the center of the fiber. Fig. 7 shows the bending loss of the diamond-core PCF at various bending radii. We observe that the loss is reduced when either the bending radius is increased or the porosity is decreased.

Effective mode area of PCFs can be calculated by using [3]

$$A_{\text{eff}} = \frac{\left[\int I(r)\, r \text{d}r\right]^2}{\left[\int I^2(r)\, \text{d}r\right]^2}, \tag{5}$$

where $I(r) = |E_t|^2$ is the transverse electric field intensity distribution in the fiber cross section. Effective area of the proposed fiber is shown in Fig. 8, where it is observed that A_{eff} is reduced with frequency and y-polarization modes show larger A_{eff} than x-polarization modes. It is also observed that the effective area is increased with porosity. The reason is that when porosity is increased, the differential index contrast between the core and the cladding is reduced, which consequently increases the amount of power spreading outside the core. Note that 40% of core porosity shows a high-birefringence with a larger mode area.

At this point, we discuss the dispersion characteristics of the proposed fiber. Material dispersion of TOPAS is ignored due to its constant refractive index and only the waveguide dispersion is calculated using dispersion parameter [17]

$$\beta_2 = \frac{2}{c}\frac{\text{d}n_{\text{eff}}}{d\omega} + \frac{\omega}{c}\frac{\text{d}^2 n_{\text{eff}}}{\text{d}\omega^2}, \tag{6}$$

where $\omega = 2\pi f$ and c is the velocity of light in vacuum. Fig. 9 shows the dispersion of the proposed PCF as a function of fre-

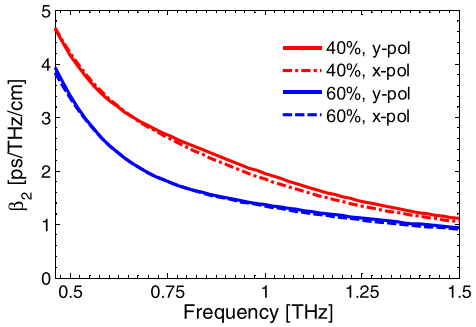

Fig. 9. Dispersion of the proposed PCF as a function of frequency at $L_{\text{core}} = 400$ μm and different porosities.

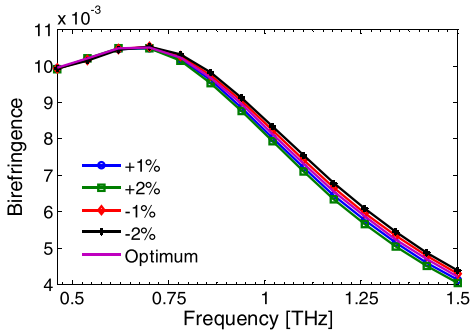

Fig. 10. Birefringence properties of the proposed fiber: optimum birefringence and effect of changing L_{core}.

quency. The dispersion within 0.48-0.82 THz at 40% porosity was 2.92 ± 0.55 ps/THz/cm. Fig. 10 shows the birefringence as a function of frequency. In the high-birefringence frequency regime of the diamond-core PCF (0.48-0.82), it shows high dispersion (Fig. 9). However, polarization dependency of the dispersion parameter is very low as observed from Fig. 10, which is convenient for highly birefringent THz transmission.

We have also examined the diamond-core fiber from the fabrication point of view. It is well known that during a standard fabrication process, $\pm 2\%$ variation may occur in the global structural parameter [18]. Owing that, we calculated the birefringence of the proposed fiber for up to $\pm 2\%$ variation of L_{core} from 400 μm as shown in Fig. 10. It can be observed from Fig. 10 that the variations in L_{core} do not affect the birefringence in the high-birefringence frequency band. We also explore the possibility of practical realization of the diamond-core PCF. In 2004, Barton *et al.* demonstrated the fabrication of microstructured polymer optical fibers (MPOFs) [19]. The method described in Ref. [19] used a combination of drilling and drawing of preforms into canes. The porous-core honeycomb bandgap fiber described in Ref. [20] has also been fabricated. Usually, air-hole patterns are drilled into the preform using a numerically controlled drill that guarantees smoother finishing and minimization of surface roughness. Therefore, this method should be sufficient for the fabrication of the proposed diamond-core structure, which would unleash the fact whether the fiber behaves similar to its numerical performance.

IV. Conclusion

We have numerically investigated a novel PCF with high-birefringence in the THz region. At optimal design parameters, the proposed fiber exhibits a birefringence $>10^{-2}$ within 0.48-0.82 THz and effective absorption loss of ~ 0.07 cm^{-1} for both the polarization modes. The three most significant properties of the diamond-core structure are its extraordinary simplicity, high-birefringence for a wide band (~ 0.34 THz) and near-zero polarization dependent loss. Thereby with proper utilization, the porous-core PCF would be a noteworthy contribution to the polarization maintaining THz technology.

References

[1] A. Hassani, A. Dupuis, and M. Skorobogatiy, "Porous polymer fibers for low-loss terahertz guiding," *Opt. Exp.*, vol. 16, no. 9, pp. 6340–6351, Apr. 2008.

[2] M. Uthman, B. M. A. Rahman, N. Kejalakshmy, A. Agarwal, and K. T. V. Grattan, "Design and characterization of low-loss porous-core photonic crystal fiber," *IEEE Photon. J.*, vol. 4, no. 6, pp. 2315–2325, Dec. 2012.

[3] S. F. Kaijage, Z. Ouyang, and X. Jin, "Porous-core photonic crystal fiber for low loss terahertz wave guiding," *IEEE Photon. Technol. Lett.*, vol. 25, no. 15, pp. 1454–1457, Aug. 1, 2013.

[4] M. B. Byrne, M. U. Shaukat, J. E. Cunningham, E. H. Linfield, and A. G. Davies, "Simultaneous measurement of orthogonal components of polarization in a free-space propagating terahertz signal using electro-optic detection," *Appl. Phys. Lett.*, vol. 98, no. 15, p. 15110, 2011.

[5] N. Karpowicz *et al.*, "Coherent heterodyne time-domain spectrometry covering the entire 'terahertz gap,'" *Appl. Phys. Lett.*, vol. 92, no. 1, p. 011131, 2008.

[6] M. Cho *et al.*, "Highly birefringent terahertz polarization maintaining plastic photonic crystal fibers," *Opt. Exp.*, vol. 16, no. 1, pp. 7–12, 2008.

[7] S. Atakaramians, S. A. Vahid, B. M. Fischer, D. Abbott, and T. M. Monro, "Low loss, low dispersion and highly birefringent terahertz porous fibers," *Opt. Commun.*, vol. 282, no. 1, pp. 36–38, 2009.

[8] R. Islam, M. S. Habib, G. K. M. Hasanuzzaman, R. Ahmad, S. Rana, and S. F. Kaijage, "Extremely high-birefringent asymmetric slotted-core photonic crystal fiber in THz regime," *IEEE Photon. Technol. Lett.*, vol. 27, no. 21, pp. 2222–2225, Nov. 1, 2015.

[9] H. Chen, D. Chen, and Z. Hong, "Squeezed lattice elliptical-hole terahertz fiber with high birefringence," *Appl. Opt.*, vol. 48, no. 20, pp. 3943–3947, 2009.

[10] N. N. Chen, J. Liang, and L.-Y. Ren, "High-birefringence, low-loss porous fiber for single-mode terahertz-wave guidance," *Appl. Opt.*, vol. 52, no. 21, pp. 5297–5302, Jul. 2013.

[11] K. Nielsen, H. K. Rasmussen, A. J. L. Adam, P. C. M. Planken, O. Bang, and P. U. Jepsen, "Bendable, low-loss Topas fibers for the terahertz frequency range," *Opt. Exp.*, vol. 17, no. 10, pp. 8592–8601, May 2009.

[12] W. Yuan, "Humidity insensitive TOPAS polymer fiber Bragg grating sensor," *Opt. Exp.*, vol. 19, no. 20, pp. 19731–19739, Sep. 2011.

[13] G. Emiliyanov *et al.*, "Localized biosensing with Topas microstructured polymer optical fiber," *Opt. Lett*, vol. 32, no. 5, pp. 460–462, 2007.

[14] A. W. Snyder and J. D. Love, *Opt. Waveguide Theory*. London. U.K.: Chapman & Hall, 1983.

[15] M. S. Habib, O. Bang, and M. Bache, "Low-loss hollow-core silica fibers with adjacent nested anti-resonant tubes," *Opt. Exp.*, vol. 23, no. 13, pp. 17394–17406, Jun. 2015.

[16] M. S. Habib, O. Bang, and M. Bache, "Low-loss hollow-core anti-resonant fibers with semi-circular nested tubes," *IEEE J. Sel. Topics Quantum Electron.*, vol. 22, no. 2, Mar./Apr. 2016, Art. no. 4402106.

[17] J. Liang, L. Ren, N. Chen, and C. Zhou, "Broadband, low-loss, dispersion flattened porous-core photonic bandgap fiber for terahertz (THz)-wave propagation," *Opt. Commun.*, vol. 295, pp. 257–261, May 2013.

[18] W. H. Reeves, J. C. Knight, P. S. J. Russell, and P. J. Roberts, "Demonstration of ultra-flattened dispersion in photonic crystal fibers," *Opt. Exp.*, vol. 10, no. 14, pp. 609–613, 2002.

[19] G. Barton, M. A. van Eijkelenborg, G. Henry, M. C. Large, and J. Zagari, "Fabrication of microstructured polymer optical fibres," *Opt. Fiber Technol.*, vol. 10, no. 4, pp. 325–335, Oct. 2004.

[20] K. Nielsen, H. K. Rasmussen, P. U. Jepsen, and O. Bang, "Porous-core honeycomb bandgap THz fiber," *Opt. Lett.*, vol. 36., no. 5, pp. 666–668, 2011.